Influence of the excitation polarization on single molecule 3D orientation imaging

Eleanor Munger, Miguel Sison, Sophie Brasselet

Influence of the excitation polarization on single molecule 3D orientation imaging

Eleanor Munger[1], Miguel Sison[1], Sophie Brasselet[1,*]

1 Aix Marseille Univ, CNRS, Centrale Marseille, Institut Fresnel, F-13013 Marseille, France

* corresponding author contact : sophie.brasselet@fresnel.fr

Abstract

Single Molecule Orientation and Localization Microscopy (SMOLM) is gaining an increasing interest in the community of localization microscopy, due to the capability to monitor orientational information in addition to spatial reconstruction. In many cases, molecule's orientations are not random and their linker to a protein of interest is sufficiently rigid to be able to report orientation information from this protein. While several strategies exist to report single molecule orientation based on polarization splitting and point spread function engineering, the effect of the incident polarization has been often neglected by supposing its effect embeded in the retrieved angular parameters, or by supposing the excitation to be isotropic or the rotational diffusion to be very fast. In this work we quantify the amount of possible bias brought in SMOLM readout due to the incident polarization effect, using analytical derivations. We illustrate this effect experimentally on single molecules attached to a surface in presence of wobbling.

Introduction

Determination of molecular orientation at the single molecule level for Single Molecule Orientation and Localization Microscopy (SMOLM) is a rapidly developing field in the super-resolution imaging community, which goal is to retrieve dipolar 3D orientation information from polarized Single Molecule Localization Microscopy (SMLM). Models have been developed to provide a formalism of the vectorial propagation of fluorescent radiating dipoles in microscopy, which are widely used today in SMOLM [1],[2],[3],[4],[5] and recently extended to nonlinear optical processes [6]. Models in SMOLM imaging however most often suppose that for every orientation, the molecule is excited in the same way. This supposes that either the excitation polarization is totally isotropic, or that the molecule rotates much faster than its fluorescence lifetime and within a manner that its emitted photon is emitted from a molecular orientation completely decorrelated from that of its excited state.

In reality, excitation polarizations commonly used in microscopy are not incoherent and isotropic, and the rotational diffusion rates of single molecules are not precisely known, in particular when they are attached to a protein or themself of large sizes, such as fluorescent proteins, or within cell membranes. Rotational dynamics can be variable depending on factors such as the labelling linker structure and the charge/steric properties of the environment [7]. In isotropic solutions, typical rotational diffusion rates of single molecules are faster than the fluorescence lifetime (typically a few ns), however it increases by up to an order of magnitude in viscous solutions, membranes [8] and in the cell cytoplasm, as well

as when attached to a surface [9][10] or when the fluorophore is a fluorescent protein [11]. Rotational motion of single molecules has shown to affect localization precision in single molecule localization microscopy (SMLM), in particular for fixed molecules which point spread function (PSF) can be strongly deformed [12]. In polarized single molecule detection, whose goal is to measure the molecule's orientation and localization, the measurement is affected by rotational motion. First, if rotational molecular diffusion occurs at time scales slower than the fluorescence lifetime τ_f (but still faster than the integration time of the camera, typically ~20-100ms), particular orientations that lie along this excitation direction will be favored more than others. Second, in situations where molecular angular fluctuations are faster than τ_f (still within angular limits imposed by their angular distribution) then this distribution, being oriented, is sensitive to the excitation polarization in a manner specific to its main orientation. Bias induced by rotational motion in single molecule orientation and localization microscopy (SMOLM) is often ignored supposing fast rotational rates, or embedded in an effective anisotropy factor [13]. A recent work in lipid membranes has accounted for a known rotational motion to fit polarized SMOLM data [14]. On the other hand, modelling the effect of rotational dynamics in PSF formation imaging has been theoretically studied in several works. M. Lew et al. [12] have evaluated numerically the absorption-emission process, modelling in particular the resolution of the rotational diffusion of a dipole for a wobbling-in-cone model distribution. Stallinga et al. [15] have analytically demonstrated relevant limiting cases, making use of Legendre polynomial decomposition of the distribution function.

In this work, we follow different scenarios representative of limit rotational diffusion cases and show that retrieval of 3D orientation parameters can be, in some cases, strongly affected by the incident polarization and the angular extent of rotational diffusion. We develop a model of angle retrieval accounting for a slowly rotating dipole using higher order moments of the molecular dipole components, in contrast to a fast rotating dipole generally used in SMOLM works, which necessitates only second order moments [15]. We quantify the bias obtained on angular parameter retrieval in the case of slow rotational motion in a few configurations generally used in SMOLM imaging and finally illustrate this effect in an experimental case.

1. Modelling the effect of the incident polarization in single molecules rotational behaviors.

The principle of Single Molecule Orientation and Localization Microscopy (SMOLM) is based on the measurement of single molecule orientational readouts, which are encoded either in polarized intensities [16],[17] or in a point spread function shape [5],[18],[19],[20],[21]. In all cases, the way SMLM depends on the molecule's orientation is governed by the vectorial dependence of the dipole's emission propagation through a microscope, as extensively described in a few works [3],[15].

1.1. Point Spread Function (PSF) of oriented molecules experiencing rotational motion

In the molecular structure considered, we suppose for simplicity that the absorption and emission dipole vectors lie along the same orientation μ (different orientations can be straightforwardly deduced from the derivations below). The molecules are also supposed to explore a given angular distribution during the integration time of the camera, with a rotational diffusion time scale τ_r much

faster than this integration time. The distribution function of the absorption/emission dipole is denoted $f(\theta,\varphi)$ with $\Omega=(\theta,\varphi)$ the dipole orientation in the local frame of the distribution, denoted by the axes $(1,2,3)$ (3 being the symmetry axis of the distribution) (Figure 1a). We suppose the distribution of cylindrical symmetry and denote $\overline{\Omega}=(\rho,\eta)$ the orientation of its main axis in the (x,y,z) sample macroscopic frame. In the macroscopic frame, the dipole μ is expressed as:

$$\mu(\theta,\varphi,\rho,\eta)=R\cdot\begin{bmatrix}\sin\theta\cos\varphi\\ \sin\theta\sin\varphi\\ \cos\theta\end{bmatrix} \qquad \text{Eq. 1}$$

with $R=\begin{bmatrix}\cos\eta\cos\rho & -\sin\rho & \sin\eta\cos\rho\\ \cos\eta\sin\rho & \cos\rho & \sin\eta\sin\rho\\ -\sin\eta & 0 & \cos\eta\end{bmatrix}$ the rotation matrix between the local distribution frame and the macroscopic frame.

The incident electric field defining the excitation polarization is called $E=\left(E_x,E_y,E_z\right)$. The absorption probability $P_{abs}(\Omega_a)$ to absorb a photon when the molecular dipole is oriented along $\mu(\Omega_a)$ is proportional to $|\mu(\Omega_a)\cdot E|^2$. At a time *t* after this absorption event, the orientation of the dipole is Ω, which occurs within a time window of duration τ_f, the fluorescence lifetime. The emission intensity is therefore the probability to emit a photon from the dipole orientation Ω at time t while the orientation was Ω_a at time $t=0$, averaged over time during the long integration time of the camera. This process depends on $g(\Omega,\Omega_a,\mathrm{t})$, the conditional probability density function to find a dipole along Ω after its rotation from its initial position Ω_a. $g(\Omega,\Omega_a,\mathrm{t})$ is a solution to the rotational diffusion equation which was extensively described in the context of constraint fluorophores in [22],[23]. The time averaged intensity image of a single molecule is its point spread function (PSF) $I(\mathrm{r})$:

$$I(\mathrm{r})=\int_0^\infty dt\,\frac{1}{\tau_f}e^{-t/\tau_f}\int f(\Omega_a)\,P_{abs}(\Omega_a)d\Omega_a\int g(\Omega,\Omega_a,\mathrm{t})\,I_{fixed}(r,\Omega)d\Omega \qquad \text{Eq. 2}$$

Which depends on different factors:

- The first term is the probability of emission at time t after absorption $P_{em}(t)=\frac{1}{\tau_f}e^{-t/\tau_f}$.
- The second term contains $P_{abs}(\Omega_a)$, the probability of absorption at orientation Ω_a:

$$P_{abs}(\Omega_a)=|\mu(\Omega_a)\cdot\mathrm{E}|^2=\sum_{i,j=x,y,z}\langle E_i\,E_j^*\rangle\,\mu_i(\Omega_a)\,\mu_j(\Omega_a) \qquad \text{Eq. 3}$$

$\langle E_i\,E_j^*\rangle$ is the time average over all incident fields realizations, representative of its polarization coherence matrix.
Ideally in a SMOLM experiment, all molecules' orientations are excited with the same probability, avoiding photo-excitation, and the absorption probability is $P_{abs}(\Omega_a)=1$. This isotropy is often supposed in works related to SMOLM, however this situation is delicate to access in microscopy as it requires a 3D incoherent illumination.

- The third term contains $I_{fixed}(r,\Omega)$, the PSF expected from a dipole μ of fixed orientation Ω:

$$I_{fixed}(r,\Omega) = \sum_{j=x,y} \begin{bmatrix} E_j^{\mu_x}(r)^* & E_j^{\mu_y}(r)^* & E_j^{\mu_z}(r)^* \end{bmatrix} (\mu(\Omega) \cdot \mu^T(\Omega)) \begin{bmatrix} E_j^{\mu_x}(r) \\ E_j^{\mu_y}(r) \\ E_j^{\mu_z}(r) \end{bmatrix} \quad \text{Eq. 4}$$

where $E_j^{\mu_i}(r)$ is the component along j of the field radiated by μ_i, the dipole component along i.
$I_{fixed}(r,\Omega)$ can be written in a form that separates propagation and dipole terms [3],[15]:

$$I_{fixed}(r,\Omega) = \sum_{i,j=x,y,z} A_{ij}(r)\ \mu_i(\Omega)\ \mu_j(\Omega) \quad \text{Eq. 5}$$

With $A_{ij}(r) = \sum_{k=x,y} E_k^{\mu_i}(r) E_k^{\mu_j}(r)^*$

$A_{ij}(r)$ constitutes a basis of point spread functions characteristic of the radiation of dipole's contributions [3], with expressions of $E_j^{\mu_i}(r)$ that can be found from the Fourier transform of the field expressed in the pupil plane [3],[15].

The work by Stallinga [15] gives a thorough description of the calculation of Eq. (2). It has in particular emphasized that its third term is expressed in a relatively simple form:

$$\int \quad g(\Omega,\Omega_a,\mathrm{t})\ I_{fixed}(r,\Omega)d\Omega\ = I_{eq}(r,\overline{\Omega}) + \left(I_{fixed}(r,\Omega_a) - I_{eq}(r,\overline{\Omega})\right) e^{-t/\tau_r} \quad \text{Eq. 6}$$

where $I_{fixed}(r,\Omega_a)$ is the initial PSF at $t = 0$, and $I_{eq}(r,\overline{\Omega})$ is the final PSF at equilibrium ($t = \infty$) with $\overline{\Omega}$ the averaged direction reached during the molecular rotational motion:

$$I_{eq}(r,\overline{\Omega}) = \int \quad f(\Omega)\ I_{fixed}(r,\Omega)\ d\Omega\ = \sum_{i,j=x,y,z} A_{ij}(r)\ \int \quad f(\Omega)\ \mu_i(\Omega)\ \mu_j(\Omega)\ d\Omega \quad \text{Eq. 7}$$

As a result of time integration in Eq. (2), the resulting PSF can be expressed as the linear combination of fast and slow limits rotational contributions [15]:

$$I(r) = \frac{\tau_f}{\tau_f+\tau_r}\ I_{fast}(r) + \frac{\tau_r}{\tau_f+\tau_r}\ I_{slow}(r) \quad \text{Eq. 8}$$

where τ_r is the rotational diffusion time.
$I_{fast}(r)$ is a fast diffusion limit PSF, dominant for $\tau_r \ll \tau_f$, while $I_{slow}(r)$ is a slow diffusion limit PSF, dominant for $\tau_r \gg \tau_f$. In what follows, we study the influence of the excitation configuration in the two extreme cases of fast and slow diffusion, studying separately both contributions $I_{fast}(r)$ and $I_{slow}(r)$. Note that both motions still occur within a long time scale of the camera integration (~20-100ms), therefore within a constraint angular distribution function $f(\theta,\varphi)$.

$I_{fast}(r)$ is expressed as:

$$I_{fast}(r) = \int \quad f(\Omega_a)\ P_{abs}(\Omega_a) \cdot I_{eq}(r,\overline{\Omega})\ d\Omega_a \quad \text{Eq. 9}$$

where the absorption contribution appears just a multiplicative term and the integration embeds a second power dependence of the dipole components, as in $I_{eq}(r,\overline{\Omega})$ above.

$I_{slow}(r)$ is more complex as it embeds a product of both absorption probability and emission at the same orientation:

$$I_{slow}(r) = \int \quad f(\Omega_a)\, P_{abs}(\Omega_a) I_{fixed}(r,\Omega_a)\, d\Omega_a \qquad \text{Eq. 10}$$

where the integration embeds a fourth power order of the dipole components.

1.2. Fast rotational diffusion

The fast rotational contribution is:

$$I_{fast}(r) = \sum_{ij=x,y,z} \langle E_i\, E_j^* \rangle \int f(\Omega_a)\, \mu_i(\Omega_a)\mu_j(\Omega_a)\, d\Omega_a \cdot \sum_{i,j=x,y,z} A_{ij}(r) \int f(\Omega)\, \mu_i(\Omega)\, \mu_j(\Omega)\, d\Omega$$

$$I_{fast}(r) = \sum_{ij=x,y,z} \langle E_i\, E_j^* \rangle \langle \mu_i\, \mu_j \rangle \cdot \sum_{ij=x,y,z} A_{ij}(r) \langle \mu_i\, \mu_j \rangle \qquad \text{Eq. 11}$$

Where $\langle \mu_i\, \mu_j \rangle$ is the average of the dipole components product $\mu_i\, \mu_j$ over all molecular orientations, expressed as a second order momentum in SMOLM works [3]. The quantities $\langle \mu_i\, \mu_j \rangle$, called second order dipole moments, express a second power dependence of the dipole components along the (x,y,z) axes averaged over the angular fluctuations. The expression of these second order moments will be detailed below.

1.3. Slow rotational diffusion

In the slow motion case,

$$I_{slow}(r) = \int f(\Omega_a) \sum_{ij=x,y,z} \langle E_i\, E_j^* \rangle\, \mu_i(\Omega_a)\mu_j(\Omega_a) \sum_{i,j=x,y,z} A_{ij}(r)\ \mu_i(\Omega_a)\, \mu_j(\Omega_a)\, d\Omega_a$$

$$I_{slow}(r) = \sum_{ij,k,l=x,y,z} \langle E_k\, E_l^* \rangle\, A_{ij}(r) \cdot \langle \mu_i\, \mu_j\, \mu_k\, \mu_l \rangle \qquad \text{Eq. 12}$$

Here $\langle \mu_i\, \mu_j\, \mu_k\, \mu_l \rangle$ is the orientational average of a fourth power dipole component, called fourth order dipole moment.

The general expression of the PSF from oriented single molecules written in Eq. (8) therefore becomes a decomposition over the PSF basis $A_{ij}(r)$:

$$I(r) = \sum_{ij=x,y,z} A_{ij}(r) \cdot \left(\frac{\tau_f}{\tau_f+\tau_r} m_{ij}^{fast} + \frac{\tau_r}{\tau_f+\tau_r} m_{ij}^{slow} \right) \quad \text{Eq. 13}$$

With m_{ij} the dipole moments involved in the decompositions:

$$m_{ij}^{fast} = \left[\sum_{k,l=x,y,z} \langle E_k \, E_l^* \rangle \, \langle \mu_k \, \mu_l \rangle \right] \cdot \langle \mu_i \, \mu_j \rangle \quad \text{Eq. 14}$$

$$m_{ij}^{slow} = \sum_{k,l=x,y,z} \langle E_k \, E_l^* \rangle \, \langle \mu_i \, \mu_j \, \mu_k \, \mu_l \rangle \quad \text{Eq. 15}$$

Note that an ideal incoherent 3D illumination called 'isotropic' leads to the same dependence of m_{ij} on the dipole contributions: $I_{fast}(r) = I_{slow}(r) = \sum_{ij=x,y,z} A_{ij}(r) \cdot m_{ij}^{iso}$, with:

$$m_{ij}^{iso} = \langle \mu_i \, \mu_j \rangle \quad \text{Eq. 16}$$

This situation is generally assumed in SMOLM studies.

The relation between these moments and the orientational parameters of the dipole are described by displaying the PSF resulting from different rotational dynamics and excitation polarizations situations. We investigate realistic excitation polarization cases that are typically used in SMLM imaging, whose expressions for the incident field E are detailed here:

- The most used illumination is Total Internal Reflexion (TIRF), which advantageously decreases the fluorescence background by a confinement of the light intensity at the proximity of the coverslip. We suppose a tilted incidence angle θ_i in the plane (x, z) at the interface between the coverslip (refractive index n_1) and a medium (refractive index n_2). This leads to an incident field of the form[24]:

$$\left(E_x^{TILT}, E_y^{TILT}, E_z^{TILT}\right) = \left(\frac{2cos\theta_i \left(sin^2\,\theta_i - n^2\right)^{1/2} e^{-i(\delta_p+\pi/2)}}{(n^4\,cos^2\,\theta_i + sin^2\,\theta_i - n^2)^{1/2}} E_p, \frac{2cos\theta_i e^{-i(\delta_s)}}{(1-n^2)^{1/2}} E_s, \frac{2cos\theta_i sin\theta_i e^{-i(\delta_p+\pi/2)}}{(n^4\,cos^2\,\theta_i + sin^2\,\theta_i - n^2)^{1/2}} E_p \right) \quad \text{Eq. 17}$$

with $n = n_2/n_1$. E_p and E_s are the incident field polarization components along the p and s polarization directions, and $\theta_{i,TIRF} = \text{asin}(n_2/n_1)$ at the TIRF condition. δ_p and δ_s are the fields phase shifts at the interface with $\delta_p = atan\left[\frac{\left(sin^2\,\theta_i - n^2\right)^{1/2}}{n^2 cos\theta_i}\right]$ and $\delta_s = atan\left[\frac{\left(sin^2\,\theta_i - n^2\right)^{1/2}}{cos\theta_i}\right]$.

- At normal incidence, the most homogeneous polarization is reached by circular polarization, which nevertheless cancels all photo-excitation along the axial direction:

$$\left(E_x^{CIRC}, E_y^{CIRC}, E_z^{CIRC}\right) = E_0 \, (1, i, 0) \quad \text{Eq. 18}$$

- Another extreme case is the strongly polarized photo-excitation obtained from a normal incidence, linearly polarized in the sample plane:

$$\left(E_x^{LIN}, E_y^{LIN}, E_z^{LIN}\right) = E_0\,(\cos\alpha\,, \sin\alpha\,, 0) \qquad \text{Eq. 19}$$

  The resulting absorption probability $P_{abs}(\Omega_a) = |\mu(\Omega_a) \cdot \mathrm{E}|^2$, being the result of the projection of the molecular dipole on the electric field, is therefore strongly anisotropic along this electric field direction.

Figure 1 depicts the resulting PSF obtained for two specific molecular orientational behaviors, in the case of four illumination conditions illustrated in Figure 1b: (i) isotropic illumination (both fast and slow contributions to the PSF giving similar situations), (ii) TIRF, (iii) linearly polarized along x ($\alpha = 0°$) at normal incidence and (iv) circularly polarized at normal incidence. We purposefully chose molecular orientational situations where the effect of the photo-excitation was strong. The parameters of the distribution functions used for this model are plotted in Figure 1a. The molecular dipole is supposed to wobble in a cone which defines the shape of the distribution function $f(\Omega)$ of aperture δ, oriented along the mean direction $\overline{\Omega} = (\rho, \eta)$. $f(\Omega)$ is defined by a uniform distribution of molecular orientations inside this cone.
Figure 1c represents the case of a quite large wobbling angle $\delta = 100°$, oriented in the sample plane ($\eta = 90°$) in the direction ($\rho = 30°$) relative to x. While the isotropic illumination / fast dipole rotation case ($\tau_r \ll \tau_f$) results in a PSF which is almost symmetric as expected from the exploration of a wide range of angles, the TIRF illumination and slow motion hypothesis leads to a PSF that almost resembles that of a fixed dipole oriented along z. This is confirmed by the shape of the PSF projected along two perpendicular directions (denoted 0° and 90° in Figure 1c). The reason for this strong PSF deformation is the strong component of the axial contribution of the TIRF incident field, which, in the case of a slow motion ($\tau_r \gg \tau_f$), favours the dipole directions along z within the distribution function. In the case of intermediate situations where $\tau_r \approx \tau_f$, the PSF is expected to be a linear combination of the fast motion PSF described above and this structured PSF, with relative weights expressed in Eq. (13). In other situations such as in-plane linear and circular, the slow limit PSF is not very different from the isotropic/fast limit PSF, which is expected from the in-plane orientation of the molecular distribution.
Figure 1d shows similar simulations in the case of a PSF oriented close to the axial direction ($\eta = 5°, \rho = 30°$) with a relatively small wobbling angle $\delta = 50°$. In this situation, an opposite effect appears as compared to in-plane distributions: the TIRF illumination slightly deforms the PSF by mimicking a fixed dipole along z, while the in-plane illumination forces the PSF to resemble that of a distribution in the plane of the sample. Here again, a slow motion is seen to have a detrimental effect on the resulting PSF shape, potentially biasing any strategy based on PSF engineering in particular.

Figure 1 finally illustrates the potentially strong effect of a tilted photo-excitation on the PSF deformation. In particular, all methods based on PSF engineering would lead to strongly biased results in this situation.

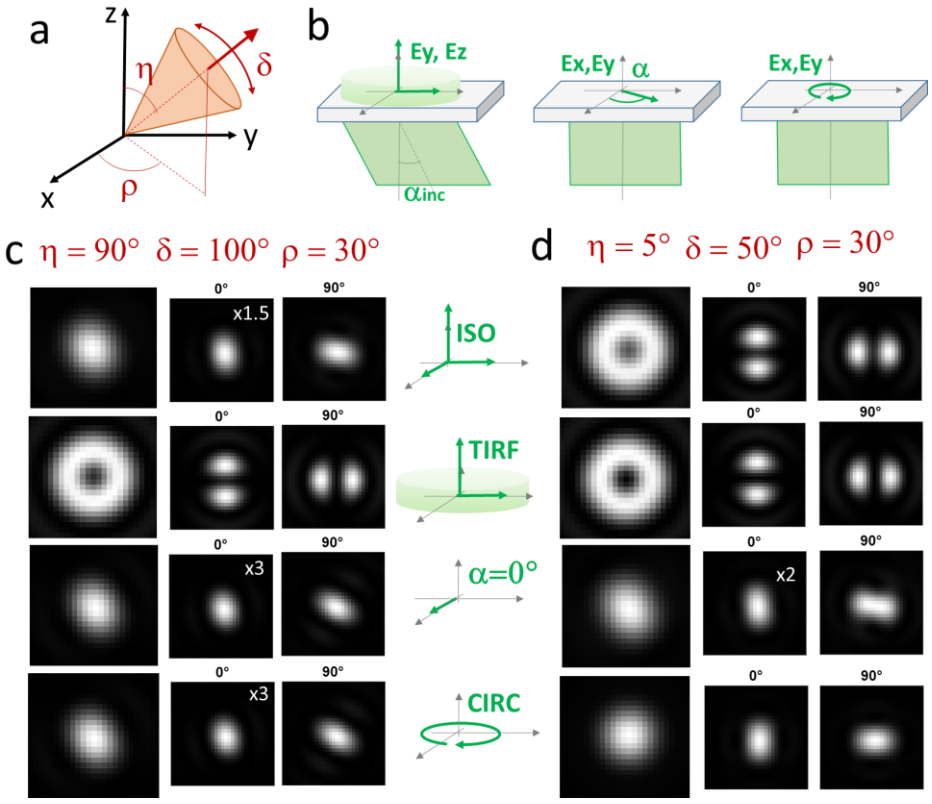

Figure 1. Point spread function of single molecules in different cases of rotational diffusion and excitation polarizations. (a) Notations used to represent the orientational behaviour of single molecules experiencing rotational diffusion within a cone: (ρ, η) are the azimuthal and elevation angles of the main axis of the cone respectively, and δ is the cone aperture. (b) Different illumination conditions considered in this work: tilted illumination (incidence angle θ_i) using a p incident polarization, normal incidence using a rotating incident linear polarization (angle α relative to x) or circular polarization. (c) Theoretical Point Spread Functions (PSF) of a single molecule in the image plane, simulated using different illumination conditions from top to bottom: ISO (isotropic depolarized excitation, also mimicking a freely rotating molecule), TIRF (tilted illumination at the total internal reflection angle, p polarized), and two normal-incidence conditions of different input polarizations (linear and circular). The molecular orientation condition (ρ =30°, η = 90°, δ = 100°) is representative of a highly wobbling in-plane molecule. (d) Similar simulations under the molecular orientation conditions: (ρ =30°, η = 5°, δ = 50°), representative of a moderately wobbling out of plane molecule. Parameters used for the microscope objective, coverslip and medium: $NA = 1.45,\ n_2 = 1.33$, $n_1 = 1.5$.

Below we illustrate how the resulting moments are affected by the presence of a slow motion in different cases of illumination conditions. Since these moments are key ingredients measured in SMOLM for the retrieval of molecules' orientation parameters, quantifying the bias induced by the incident polarization excitation on these moments is a relevant signature of sources of bias in any SMOLM experiment, whatever its implementation (polarization splitting or PSF engineering).

2. Molecular second order moments

Eq. (13) shows that the PSF is formed from the linear combination of bases PSF terms $A_{ij}(r)$ and the dipole moments m_{ij}, which take different forms depending on the rotational diffusion rate of the molecule. Below, we show how these moments are affected by the illumination conditions and provide a way to retrieve the orientational parameters of the molecule (ρ, η, δ) in the case of known illumination and rotational rates.

2.1. Fast rotational diffusion

In the case of molecules rotating much faster than their fluorescence life time scale, there is no correlation between the angle of the absorption dipole and that of the emission dipole. The two events are decorrelated and $m_{ij}^{fast} = \langle P_{abs} \rangle \langle \mu_i \mu_j \rangle$, therefore the absorption cross section plays only a role of a homogeneous efficiency factor. In the case of a distribution of cone shape defined by the parameters (ρ, η, δ), the dipole moment terms m_{ij} write:

$$m_{ij}^{fast}(\rho, \eta, \delta) = \langle P_{abs} \rangle (\rho, \eta, \delta) \; . \; \int_0^{2\pi} d\varphi \int_0^{\delta/2} d\theta \; \sin\theta \; \mu_i \mu_j (\theta, \varphi, \rho, \eta) \qquad \text{Eq. 20}$$

with $\langle P_{abs} \rangle = \int_0^{2\pi} d\varphi \int_0^{\delta/2} d\theta \; \sin\theta \; f(\theta, \varphi) \, P_{abs}(\theta, \varphi, \rho, \eta)$ which also depends on the orientation and width of the molecular angular distribution.
The moments m_{ij} can be written in a simple form when expressed in the frame of the distribution function (1,2,3). Since $\mu_i = \sum_{u=1,2,3} R_i^u(\rho, \eta) \; \mu_u(\theta, \varphi)$:

$$\mu_i \; \mu_j (\theta, \varphi, \rho, \eta) = \sum_{u,v=1,2,3} R_{ij}^{uv}(\rho, \eta) \; \mu_u \mu_v (\theta, \varphi) \qquad \text{Eq. 21}$$

R_{ij}^{uv} is the second order rotation product $R_{ij}^{uv}(\rho, \eta) = (i.u)(j.v)(\rho, \eta)$, with $(i, j) = (x, y, z)$ and $(u, v) = (1,2,3)$. Therefore:

$$m_{ij}^{fast}(\rho, \eta, \delta) = \langle \mu_i \mu_j \rangle = \langle P_{abs} \rangle (\rho, \delta, \eta) . \sum_{uv=1,2,3} R_{ij}^{uv} \; (\rho, \eta) \; m_{uv} \; (\delta) \qquad \text{Eq. 22}$$

With $m_{uv} = \langle \mu_u \mu_v \rangle$ with $(\mu_1, \mu_2, \mu_3) = (\sin\theta \cos\varphi \, , \sin\theta \sin\varphi, \cos\theta)$.
If the molecular distribution is of cylindrical symmetry, all off diagonal terms m_{uv} vanish and only diagonal terms are expressed as functions of the distribution function parameters. In a cone model, this leads to only three non-vanishing elements:

$$\begin{bmatrix} m_{11} \\ m_{22} \\ m_{33} \end{bmatrix} = \begin{bmatrix} \langle \mu_1^2 \rangle = \frac{2}{3} . \left(2 + \cos\frac{\delta}{2}\right)\left(1 - \cos\frac{\delta}{2}\right) \\ \langle \mu_2^2 \rangle = \langle \mu_1^2 \rangle = \frac{2}{3} . \left(2 + \cos\frac{\delta}{2}\right)\left(1 - \cos\frac{\delta}{2}\right) \\ \langle \mu_3^2 \rangle = \frac{1}{3} . \left(1 - \cos^3\frac{\delta}{2}\right) / \left(1 - \cos\frac{\delta}{2}\right) \end{bmatrix} \qquad \text{Eq. 23}$$

The macroscopic frame components m_{ij}^{fast} are therefore finally expressed as:

$$\begin{bmatrix} m_{xx} \\ m_{yy} \\ m_{zz} \\ 2.m_{xy} \\ 2.m_{xz} \\ 2.m_{yz} \end{bmatrix} = \langle P_{abs} \rangle(\rho,\eta,\delta) \,. \begin{bmatrix} \cos^2\eta\cos^2\rho & \sin^2\rho & \sin^2\eta\cos^2\rho \\ \cos^2\eta\sin^2\rho & \cos^2\rho & \sin^2\eta\sin^2\rho \\ \sin^2\eta & 0 & \cos^2\eta \\ \cos^2\eta\sin 2\rho & -\sin 2\rho & \sin^2\eta\sin 2\rho \\ -\sin 2\eta\cos\rho & 0 & \sin 2\eta\cos\rho \\ -\sin 2\eta\sin\rho & 0 & \sin 2\eta\sin\rho \end{bmatrix} \begin{bmatrix} m_{11} \\ m_{22} \\ m_{33} \end{bmatrix} \quad \text{Eq. 24}$$

2.2. Slow rotational diffusion

In the case of molecules rotating much slower than their fluorescence life time (but still faster than the camera integration time), $m_{ij}^{slow} = \langle P_{abs} \cdot \mu_i \mu_j \rangle$. If the distribution is the shape of a cone:

$$m_{ij}^{slow}(\rho,\eta,\delta) = \sum_{k,l=x,y,z} \langle E_k \, E_l^* \rangle \int_0^{2\pi} d\varphi \int_0^{\delta/2} d\theta \, \sin\theta \, \mu_i \, \mu_j \, \mu_k \, \mu_l(\theta,\varphi,\rho,\eta) \quad \text{Eq. 25}$$

Similarly as above, the moments $m_{ijkl} = \langle \mu_i \mu_j \mu_k \mu_l \rangle$ can be expressed in a simple form when expressed in the frame of the distribution function (1,2,3). Since $\mu_i = \sum_{u=1,2,3} R_i^u(\rho,\eta) \, \mu_u(\theta,\varphi)$:

$$\mu_i \, \mu_j \, \mu_k \, \mu_l(\theta,\varphi,\rho,\eta) = \sum_{s,t,u,v=1,2,3} R_{ijkl}^{stuv}(\rho,\eta) \, \mu_s \mu_t \mu_u \mu_v(\theta,\varphi) \quad \text{Eq. 26}$$

R_{ijkl}^{stuv} is the fourth order rotation product $R_{ijkl}^{stuv}(\rho,\eta) = (s \cdot i)(t \cdot j)(u \cdot k)(v \cdot l)(\rho,\eta)$, with $(i,j,k,l) = (x,y,z)$ and $(s,t,u,v) = (1,2,3)$. Therefore:

$$m_{ij}^{slow}(\rho,\eta,\delta) = \sum_{k,l=x,y,z} \langle E_k \, E_l^* \rangle \sum_{s,t,u,v=1,2,3} R_{ijkl}^{stuv}(\rho,\eta) \; m_{stuv}(\delta) \quad \text{Eq. 27}$$

With the components of $m_{stuv}(\delta)$ calculated as :

$$\begin{bmatrix} m_{1111} \\ m_{2222} \\ m_{3333} \\ m_{1122} \\ m_{1133} \\ m_{2233} \end{bmatrix} = \begin{bmatrix} \langle \mu_1^4 \rangle = \frac{1}{10}.\left(19 + 18\,\cos\frac{\delta}{2} + 3\cos\delta\right)\left(1-\cos\frac{\delta}{2}\right)^2 \\ \langle \mu_2^4 \rangle = \langle \mu_1^4 \rangle = \frac{1}{10}.\left(19 + 18\,\cos\frac{\delta}{2} + 3\cos\delta\right)\left(1-\cos\frac{\delta}{2}\right)^2 \\ \langle \mu_3^4 \rangle = \frac{1}{5}.\left(1-\cos^5\frac{\delta}{2}\right)/\left(1-\cos\frac{\delta}{2}\right) \\ \langle \mu_1^2\mu_2^2 \rangle = \frac{1}{3}.\langle \mu_1^4 \rangle = \frac{1}{30}.\left(19 + 18\,\cos\frac{\delta}{2} + 3\cos\delta\right)\left(1-\cos\frac{\delta}{2}\right)^2 \\ \langle \mu_1^2\mu_3^2 \rangle = \frac{1}{60}.\left(4 + \cos^3\frac{\delta}{2}(-7 + 3\cos\delta)\right)/\left(1-\cos\frac{\delta}{2}\right) \\ \langle \mu_2^2\mu_3^2 \rangle = \langle \mu_1^2\mu_3^2 \rangle = \frac{1}{60}.\left(4 + \cos^3\frac{\delta}{2}(-7 + 3\cos\delta)\right)/\left(1-\cos\frac{\delta}{2}\right) \end{bmatrix} \quad \text{Eq. 28}$$

In the case of a slow rotational motion, the resulting dipole moments are therefore not only more complex dependencies of the parameters (ρ,η,δ), they also depend on the incident field polarization through the factors $\langle E_k \, E_l^* \rangle$.

2.3. Effect of the rotational diffusion on the measured quantities in SMOLM

In order to emphasize the role of the excitation polarization in SMOLM, we depict the dependence of the dipole momentum values m_{ij} using normalized factors:

$$P_{xy} = \frac{m_{xx} - m_{yy}}{M},\ P_{zz} = \frac{m_{zz}}{M},\ P_{uv} = \frac{2m_{xy}}{M}$$

$$P_{yz} = \frac{2M_{yz}}{M} \text{ and } P_{xz} = \frac{2M_{xz}}{M} \qquad \text{Eq. 29}$$

with the norm $M = m_{xx} + m_{yy} + m_{zz}$.
These polarization factors are reminiscent of the Stokes parameters describing polarization states in paraxial optics. Importantly, the P factors report in a relatively simple way the orientational characteristics of single molecules. In the isotropic illumination/fast rotational diffusion case, there is indeed a very direct relation between polarization factors and angle parameters:

$$P_{xy} = \big(1 - 3\lambda(\delta)\big)\sin^2\eta\cos 2\rho;\ P_{uv} = \big(1 - 3\lambda(\delta)\big)\sin^2\eta\sin 2\rho$$

$$P_{zz} = \big(1 - 3\lambda(\delta)\big)\ \cos^2\eta + \lambda(\delta)$$

$$P_{xz} = \big(1 - 3\lambda(\delta)\big)\sin 2\eta\cos\rho;\ P_{yz} = \big(1 - 3\lambda(\delta)\big)\sin 2\eta\sin\rho \qquad \text{Eq. 30}$$

with $\lambda(\delta) = \frac{\left(1-\cos\left(\frac{\delta}{2}\right)\right)\left(2+\cos\left(\frac{\delta}{2}\right)\right)}{6}$.

Eq. (30) shows that the $(P_{xy},\ P_{uv})$ couple of parameter is mostly sensitive to the in-plane orientation of the molecular distribution (ρ), while the P_{zz} parameters is sensitive to the off-plane orientation (η), independently on (ρ), All parameters also depend on (δ), with a decrease of $P_{xy}^2 + P_{uv}^2$ with δ.

Note that in this isotropic illumination / fast rotation case, all parameters (ρ, η, δ) can be retrieved through simple equations:

$$\tan 2\rho = \frac{P_{uv}}{P_{xy}};\ \tan^2\eta = \frac{P_{xy}^2 + P_{uv}^2}{P_{xz}^2 + P_{yz}^2}$$

$$\lambda(\delta) = P_{zz} + \sqrt{P_{xy}^2 + P_{uv}^2}$$

$$\cos\eta = \sqrt{\frac{P_{zz} - \lambda(\delta)}{\lambda(\delta) - 1}} \qquad \text{Eq. 31}$$

Figures 2 and 3 depict the dependence of $(P_{xy},\ P_{uv},\ P_{zz})$ on the different illumination conditions. $(P_{xz},\ P_{yz})$ are omitted in what follows, since their only added value is to provide a phase information on the (ρ, η) direction pointed by the time-averaged dipole. In the scatter plots of Figs. 2 and 3, each marker corresponds to a given set of angle values (ρ, η, δ). A marker (e.g. a given (ρ, η, δ) value) is

represented by its corresponding $(P_{xy},\ P_{uv},\ P_{zz})$ values, deduced from Eq. (30). From these P values, Each marker is thus positioned in a scatter plot with $(P_{xy},\ P_{uv},\ P_{zz})$ axes, and its color encodes its corresponding δ value. In Fig. 2a, all $(P_{xy},\ P_{uv})$ accessible values from all (ρ, η, δ) values are depicted in a $(P_{xy},\ P_{uv})$ plot. The center region at $(P_{xy} \sim 0,\ P_{uv} \sim 0)$ values contains visibly yellow markers only, sign of very high δ values (which is expected from close to isotropic distributions $\delta \sim 180°$), while the extreme $(P_{xy} \sim \pm 1,\ P_{uv} \sim \pm 1)$ values correspond to blue markers, e.g. low δ values corresponding to almost fixed dipoles. The rest of the space is filled with markers corresponding to all possible (ρ, η, δ) values. Similarly, Figs. 2(b-c) depicts the position of all possibly measured couples $(P_{xy},\ P_{zz})$ (Fig. 2b), and $(P_{uv},\ P_{zz})$ (Fig. 2c). All $(P_{xy}, P_{uv},\ P_{zz})$ values are comprised in a cone which surface contains the values of the extreme fixed dipole case $\delta \sim 0°$.

Figures 2(d-f) shows the same representation for a linear incident polarization along x provided by a normal incidence illumination, under the condition of a slow rotational motion. This situation displaces the distribution of measured $(P_{xy}, P_{uv},\ P_{zz})$ values towards higher P_{xy}, since the dipole moment m_{xx} predominates as a result of the important photo-excitation along the x direction. Similarly, this distribution is displaced along higher or lower (P_{xy}, P_{uv}) values for a linear polarization angle α along 45°,90° or 135° (Fig. 2b). This representation illustrates how strongly these factors can be biased, upon linearly incident polarization illumination.

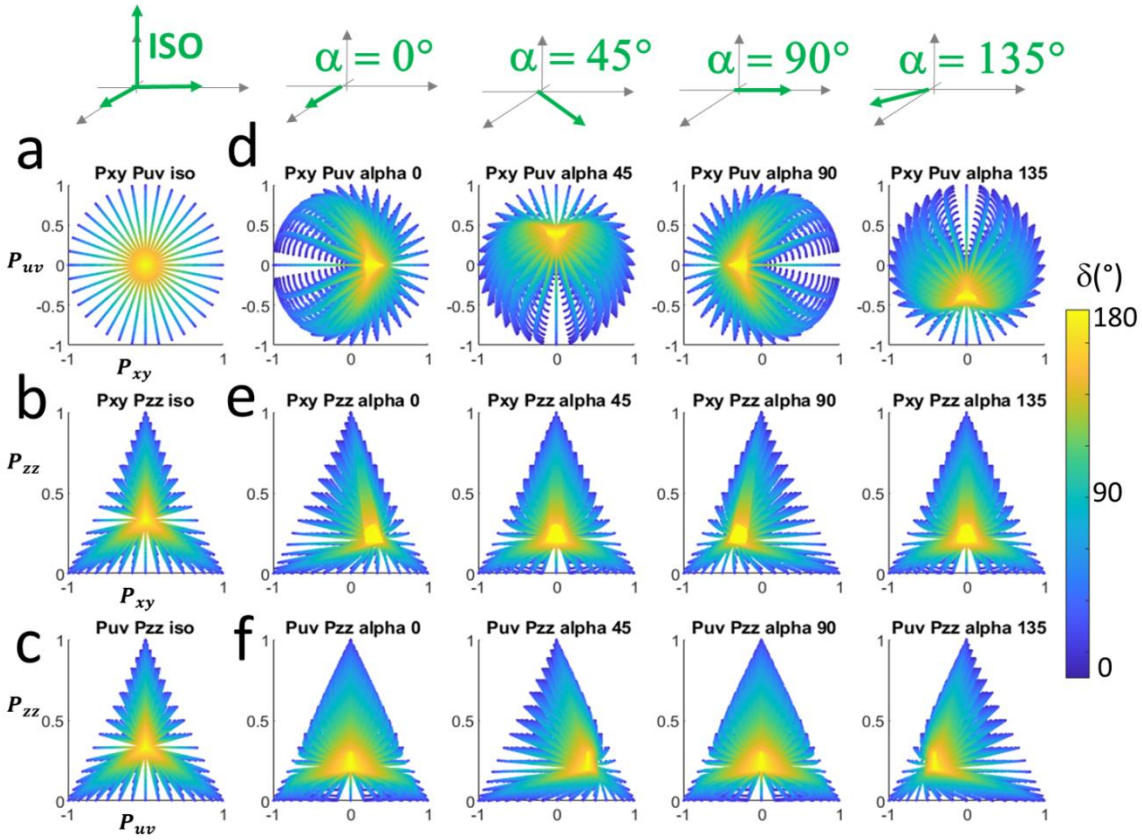

Figure 2. Dependence of the values of P_{xy}, P_{uv} and P_{zz} for all possible single molecule orientation conditions (ρ, η, δ) with δ encoded in color. The plotted horizontal axis and vertical axis quantities are indicated at the top of each graph. (a-c) case of an isotropic illumination / fast rotational motion. (d-f) case of particular photo-excitations, under slow rotational motion conditions. a) shows P_{xy}, P_{uv} values; b) P_{xy}, P_{zz} values and c) P_{uv}, P_{zz} values. (d-f) similar representation for a normal incidence, in-plane

linearly polarized excitation with an incident polarization angle a varying from 0 to 135° (indicated at the top of the columns).

Figure 3(a-c) depicts a similar information, for an incident circular polarization under normal incidence. A direct comparison with the isotropic situation (Fig. 2(a-c)) shows that high δ values lead to biased determination of the (P_{xy}, P_{uv}, P_{zz}) factors, with a slight over-estimation of (P_{xy}, P_{uv}) and an under-estimation of P_{zz} which results from the absence of longitudinal component of the field.

The case of a tilted incident illumination (p polarized) is shown in Fig. 3(d-f), which shows that the increase of the tilt permits to better balance the (P_{xy}, P_{uv}) contribution, leading to less bias in their determination, as a result of the (x, y) contributions of the electric field of excitation. However a higher tilt, towards TIRF illumination, leads to a higher axial component of the incident field, which leads to an over-estimation of the P_{zz} factor. As a result, the determination of the off-plane orientation of the molecules η is likely to be under-estimated.

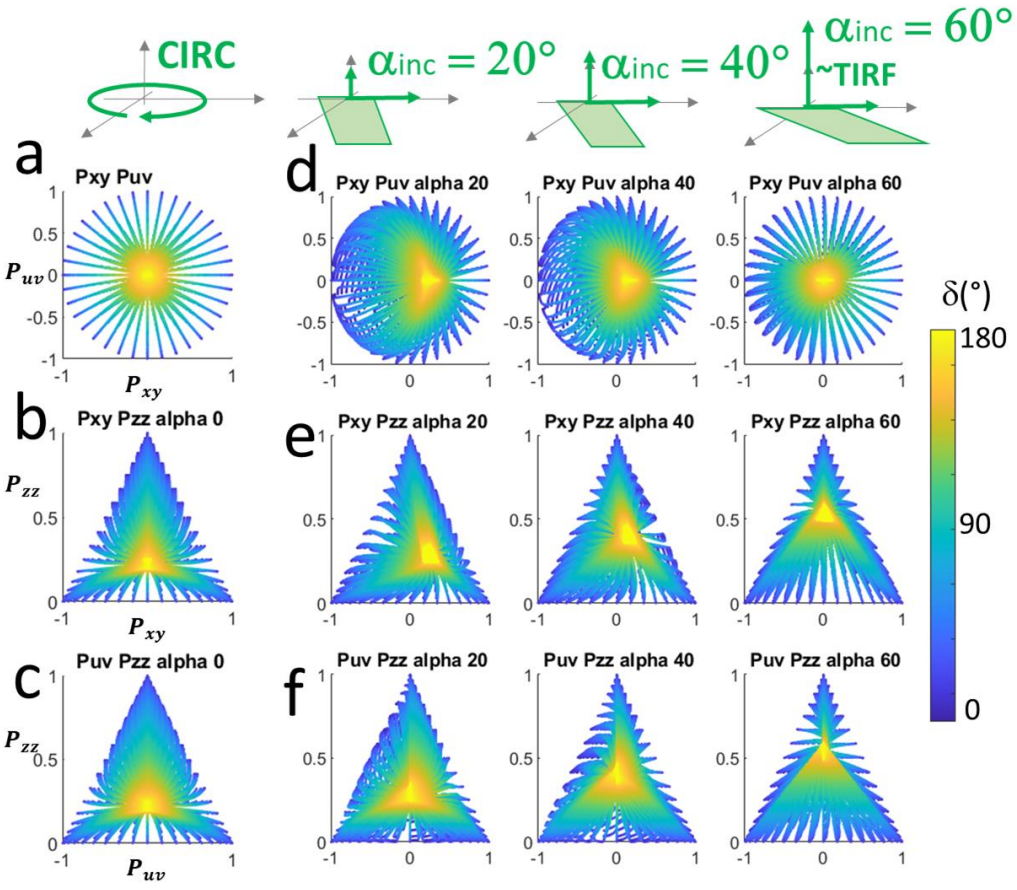

Figure 3. Dependence of the values of P_{xy}, P_{uv} and P_{zz} for all possible single molecule orientation conditions (ρ, η, δ) with δ encoded in color. The plotted horizontal axis and vertical axis quantities are indicated at the top of each graph. (a-c) case of a normal incidence, circularly polarized illumination. a) shows P_{xy}, P_{uv} values; b) P_{xy}, P_{zz} values and c) P_{uv}, P_{zz} values. (d-f) similar representation for different cases of incidence : slightly tilted (θ_i = 20°), tilted (θ_i = 40°), to close to TIRF (θ_i = 60°). The illumination conditions are indicated at the top of the columns.

3. From molecular moments to microscopy imaging of single oriented molecules.

As can be seen in the previous derivations, the angular parameters (ρ, η, δ) can a priori be directly extracted from the P values. In the case of an isotropic illumination / fast rotational diffusion, the use of Eq. (31) gives a direct relation for their determination (supposing that the dipole moments ca be measured with no bias). If such equations are used in the case of a slow rotational motion, a strong bias can be expected, as visibly occurring in Figs. 2,3.

Figure 4 depicts the bias expected on parameters (ρ, η, δ) if an isotropic model is used while the situation is that of a slowly rotating dipole. We define the bias as the difference between the retrieved value (using an isotropic model) and the ground truth. As expected from an ideal isotropic illumination (Fig. 4a), the retrieval shows no bias except for extreme situation where the angles are ill-defined for ρ ($\eta = 0°, \delta = 180°$). When the rotational motion is slow and the incident electric field is linearly polarized along x (Fig. 4b), a strong bias occurs at high δ values, as seen for all parameters ρ (left panel), δ (middle panel) and η (right panel), in particular at low η (off-plane molecules). In case of TIRF illumination (p polarized), the bias on ρ is even stronger. In such situation a strong bias is expected on δ at high δ values and on η at high δ values for in-plane distributions (high η) (Fig. 4c). This situation is reminiscent of the observations of Figs. 1 and 3 where under TIRF illumination, in-plane molecular distribution leads to an apparent off-plane distribution, as a result of the photo-excitation bias.

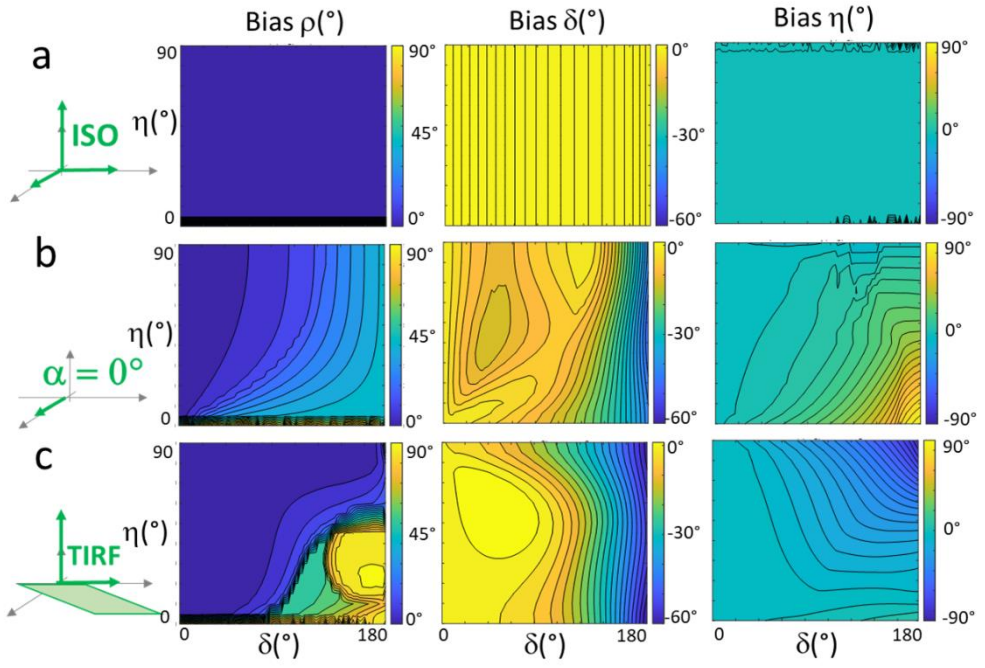

Figure 4. Bias obtained on the angular parameters ρ (left column), δ (middle column) and η (right column) under different illumination conditions : a) isotropic, b) linearly polarized along a) 0°, c) TIRF polarized along p. The bias values are represented for all possible orientation η and wobbling δ, and averaged over all possible ρ values.

To illustrate the effect of such biased situation, we suppose a collection of randomly 3D oriented molecules, such as expected from deposited molecules that can be left freely rotating within their angular distribution, fixed by the linker to the sample surface for instance. The resulting expected distributions of (ρ, η, δ) parameters are represented in histograms in Fig. 5a for an ideal isotropic / fast rotation case, where (ρ, η) span all possible orientations and the molecular wobbling is fixed to a relatively high value ($\delta = 100°$). Note that while the fast rotation case resembles a non-biased situation, all measured quantities in Eq. (24) contain as an efficiency factor the absorption probability $\langle P_{abs} \rangle(\rho, \eta, \delta)$ which is itself polarization/orientation dependent. In the case of a molecule rotating very fast within a cone, a cone oriented perpendicularly to the incident polarization will obviously not be photo-selected and thus not detectable, which induces another type of bias.

Figure 5(b-c) shows how the initially broad histograms of (ρ, η) values are considerably modified : ρ tends to be constraint to values close to the incident linear polarization as expected from the enhanced photo-excitation along this direction, while the η value histogram lacks low η populations and is enriched in in-plane $\eta \sim 90°$ value, as a result of the in-plane photo-excitation. As a result of biased (ρ, η) values, the determination of δ undergoes also a slight bias, with some departure from the expected $\delta = 100°$ wobbling. Interestingly, this situation under a lower wobbling condition $\delta = 10°$ (Fig. 5d) leads to much less bias. This is expected from the fact that the readout distribution spans less angles, therefore the effect of the photo-excitation within this distribution leads to less deformation of the apparent detected distribution.

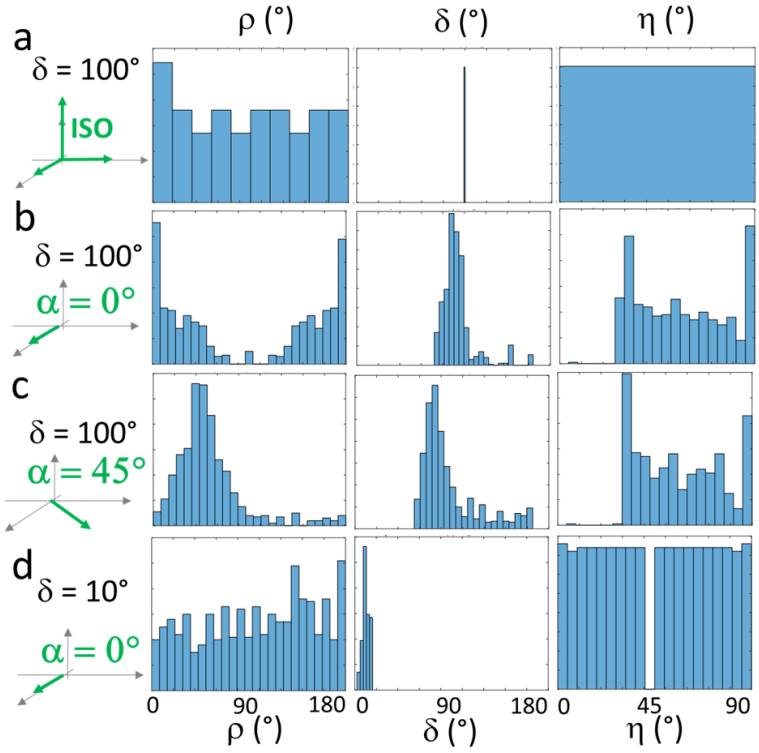

Figure 5. Histogram of retrieved values ρ (left column), δ (middle column), and η (right column) generated by the simulation of a set of randomly oriented molecules (ρ, η angles being distributed

randomly), which all have the same d wobbling angle. (a-c) δ = 100°. a) case of an isotropic illumination, b) case of a normal incidence, linear polarization along α = 0°, c) case of a normal incidence, linear polarization along α = 45°, d) case of a normal incidence, linear polarization along α = 0°, supposing a lower δ = 10°.

Similarly as for an in-plane linear polarization, tilted incidence p polarized illumination leads to a strong bias in of (ρ, η) values and some slight bias in δ for relatively high δ. This is illustrated in Fig. 6 which shows non-homogeneous histograms of ρ, biased by the input p polarization, and biased histograms of η where in-plane values $\eta \sim 90°$ are clearly lacking. A possible strategy to decrease the bias in ρ and homogenise its histogram is to use a tilted circularly polarized incidence. Unfortunately as TIRF is itself a strong polarization filter (induced by polarized selection rules at the sample interface), homogenization of the ρ histogram cannot be reached (Fig. 6b). A better homogenization can be expected by lowering the incidence angle (at the prize of a higher fluorescent background from the sample). This tilted incidence needs however to be finely tuned since a relatively lower incidence (here 40° as illustrated in Fig. 6c) leads again to a strongly biased ρ with enhanced populations along a priviledged direction. In both cases of tilted circular polarizations, the η histograms is also lacking low and high η values (Figs. 6b,c right panels), therefore η can be also biased by the lower axial contribution of the incident field.

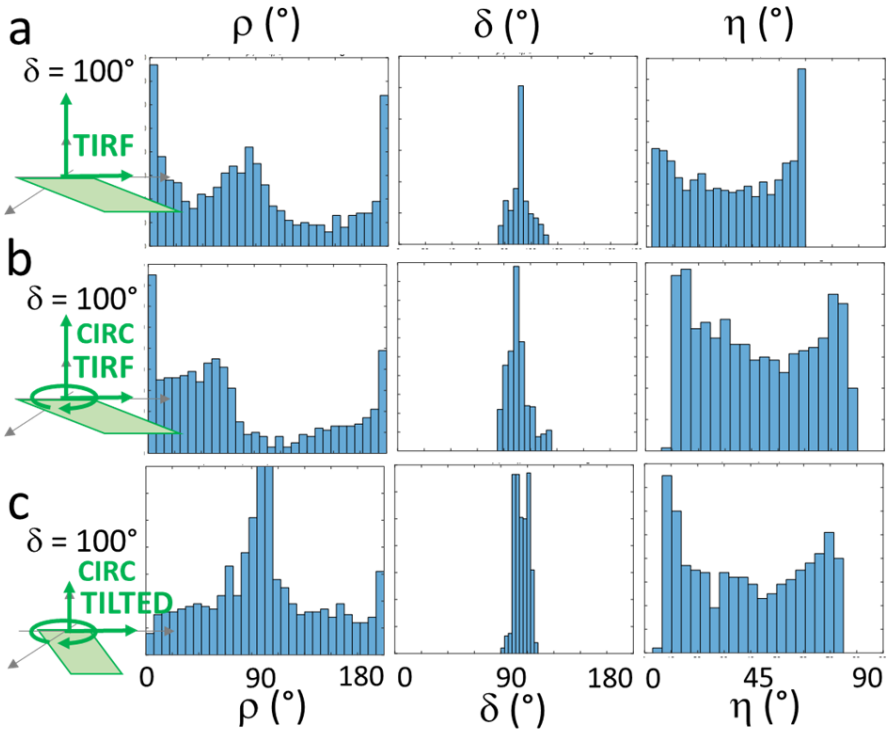

Figure 6. Histogram of retrieved values similarly as in Figure 5, supposing δ = 100°. A) case of a TIRF, p polarized illumination. B) case of TIRF, circularly polarized illumination (in the back focal plane). c) case of a tilted (θ_i = 40°), circularly polarized illumination.

At last, we performed experimental measurements of a situation mimicking the configuration simulated in Fig. 6. In order to image single fluorescent molecule attached to a coverslip in a non-rigid way, phalloidin conjugate Alexa Fluor™ 568 molecules were deposited on a coverslip treated with poly-l-lysine and left in a water environment. For this, 50 μL of poly-l-lysine was dropped and spread on a 24 mm diameter glass coverslip and let to rest for 20 mn. The coverslip was then rinsed in milli-Q water and 50 μL of 100pM phalloidin conjugate Alexa Fluor™ 568 was dropped on it and left to settle for 30 mn, this low concentration ensuring sufficient distance between isolated single molecules. Finally, the coverslip was again rinsed in milli-Q water and was placed on a glass slide with a ~0.13 mm spacer and milli-Q water in between them.

The sample was imaged using a setup recently described in [25]. The parameters (ρ, η, δ) were measured from each measured single molecule using a method based on 4-polarization projections of single molecule images, inspired from [17] with a slight modification to ensure that 3D orientation parameters can be accessed, similarly as a method developed in [26] : the method is based on the detection of 2 polarizations (projected along the 0°,90° directions) at a numerical aperture just below the critical angle (NA = 1.3) and 2 polarizations (45° and 135°) at a lower NA (NA = 1.1). This NA difference provides a detection sensitive to all (ρ, η, δ) parameters independently by the sole estimation of the integrated intensities of single molecules, independently on their PSF shape. Polarized measurements were performed on a custom built tilted incidence fluorescence inverted microscope (Nikon) with an 100x oil immersion objective (NA 1.45, Nikon). Fluorescence excitation was achieved using a continuous laser at 561 nm wavelength (Coherent) which beam was expanded and focussed at the back focal plane of the objective at a various position, providing control of the tilt incidence angle. Achromatic half and quarter wave plates (Thorlabs) were added to the incident path to control the polarization state of the incident beam. The emitted fluorescence was filtered from the excitation using a multi-edge dichroic beamsplitter (Di03-R405/488/561/635-t1, Semrock) and a multiband emission filter (ZET405/488/561/640m, Chroma). A 4-polarization detection module is mounted at the exit port of the microscope using a similar setup as in [17], except that diaphragms are placed at the back focal plane image of each path to provide different detected numerical apertures as mentioned above. In this detection module, a beam splitter is used to separate the detection path in two separate detection numerical apertures, Wollaston beam splitters and half wave plates are then used for polarization splits of each beam path, and a mirror is finally used for image recombination of the four polarized optical paths to the same camera (ORCA-Fusion C14440-20UP, Hamamatsu). All measurements were conducted using the Nikon motorized stage and Perfect Focus System (PFS) to ensure minimal sample drift. A laser power of about 80 mW was used (measured at the back focal plane of the objective) and the camera integration time was fixed at 100ms/frame with a total of 2000 frames measured. The image analysis consists in retrieving the intensity of each single molecule on four polarization channels, with a processing similar to [17] to retrieve the (P_{xy}, P_{uv}, P_{zz}) factors, from which (ρ, η, δ) parameters are deduced supposing isotropic illumination / fast rotational diffusion, following Eq. (31).

Experimental values of (P_{xy}, P_{uv}) are plotted In Fig. 7a for a collection of thousands of single molecules, in a configuration where the incident polarization excitation is set along y $(\alpha = 90°)$ at normal incidence. Visibly, the measured population does not fill a homogeneous collection of orientations as would be expected from the isotropic nature of the molecular population. This is also confirmed in the

histogram obtained for the retrieved mean orientation ρ, which shows a main population along y (Fig. 7b). If the rotation rate of single molecules would be very fast, or if the molecules would be completely fixed (e.g. very small δ), this distribution would depict a broad distribution of ρ values. The measured wobbling δ are however distributed around a mean value of δ ~ 100° (Fig. 7c), which illustrates the capacity of single molecules to rotate within a large distribution. The hypothesis of fixed immobilized dipoles is therefore excluded and the measured configuration resembles rather the case of a photo-excitation along y of a rather slowly wobbling molecule within a large cone (e.g. τ_r or same order of magnitude or larger than τ_f). This slow wobbling can be attributed to the linker between the fluorescent dipole and the coverslip, which is related to the molecular structure, but also to the charge environment which can add rotational constraint. The obtained out of plane angle η also gives a histogram with a main population around $\eta \sim 50°$ (Fig. 7d), different from the expected homogeneous wide distribution : this is attributed to the bias originating from the photo-excitation as observed in Fig. 5. This photo-excitation effect is confirmed at another angle of excitation polarization ($\alpha = 0°$) in Fig. 7e which considerably shifts the ρ histogram. At last, an attempt to limit this photo-selection by using a circular tilted incident polarization shows that the ρ histogram is enlarged but still not completely, similarly as in the simulated situation of Fig. 6c. This can be explained by the incomplete homogenization of the polarization in the plane of the sample, expected from a tilted circular polarization.

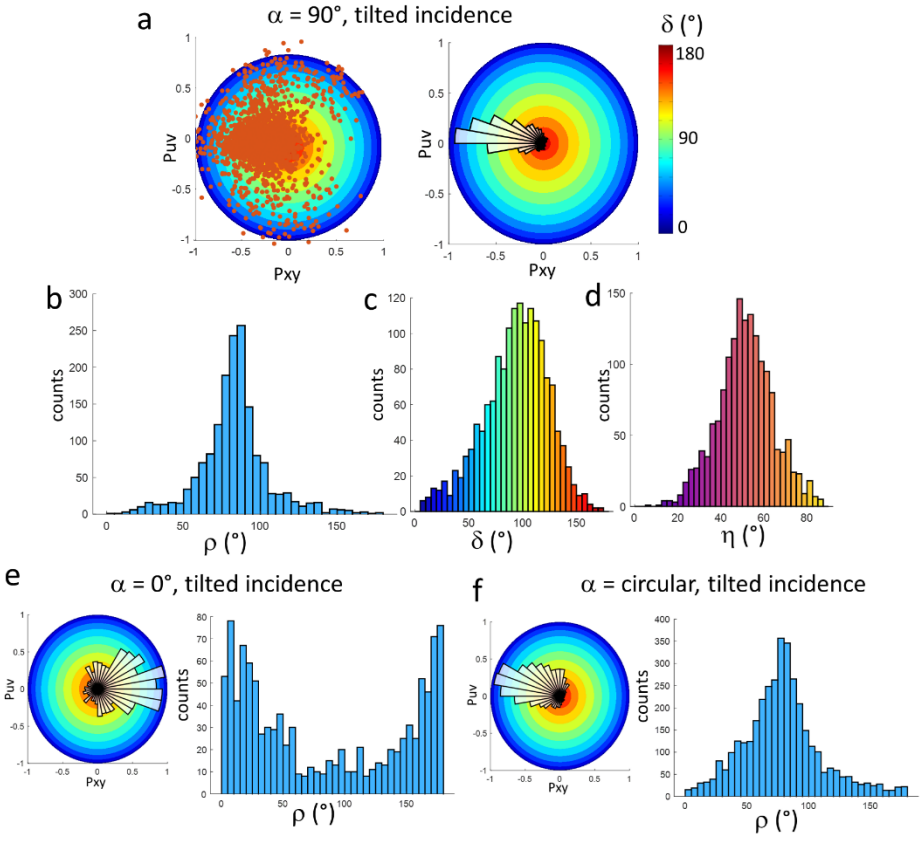

Figure 7. Data obtained from a set of thousands of single Alexa Fluor™ 568 molecules deposited on a coverslip in a water environment. The illumination is tilted (close to 40° incidence, below TIRF conditions). The detection is obtained using a 4-polarized channel setup described in the text and in [17],[25]. a) left: obtained (P_{xy}, P_{uv}) data from single molecules (red markers) depicted over the background of expected values dependent on δ (colorbar) from an isotropic illumination model. Right:

same data, represented as an angular histogram of (P_{xy}, P_{uv}) values. b) histogram of retrieved ρ values from this set of data. c) histogram of retrieved d values. d) histogram of retrieved η values. e) other set of data measured in the same tilted incidence, with a linear polarization along 0°. Left: (P_{xy}, P_{uv}) angle histogram, right : ρ histogram. f) same representation of another set of data measured in the same tilted incidence, with a circular polarization.

4. Discussion and conclusions.

Experimental results of Fig. 7 illustrate the effect of photo-selection in a *a priori* isotropic collection of single molecule's orientations. In this example, the wobbling angle of the molecules was not known *a priori* but its range could nevertheless be deduced by an average over 3D orientation measurements from the whole population measured. For slowly-rotating molecules, the obtained wobbling of about 100° is in the range of values for which the effect of photo-selection is likely to bias the in-plane orientation retrieval in SMOLM (Figs. 5,6). This is clearly illustrated in Fig.7, which shows that the rotational time of molecules is likely comparable or slower than their fluorescence life time. Indeed, while an isotropic in-plane distribution is expected, the outcome is a distribution that clearly depends on the configuration of the incident excitation. It is delicate to deduce a precise knowledge of rotational dynamics of the molecules from such data, since all parameters are mixed as shown in Eq. (13), nevertheless the example of Fig. 7 is an illustration of the possibly strong bias induced by an excitation polarization photo-selection in SMOLM measurements. Fig. 7f shows furthermore that strategies changing the input incidence angle and polarization state can aim at reducing this photo-selection effect, nevertheless the use of a tilted circular polarization does not naturally lead to an isotropic in-plane polarization due to the polarization sensitivity of interfaces.

In conclusion, we have shown a derivation of the effect of the incident excitation polarization state on the measured orientations retrieved from single molecule orientation and localization microscopy (SMOLM). Based on the decomposition of the resulting intensity into contributions that can be attributed to a slow and a fast limit PSFs, we have shown that both limits can be simply translated into dipole moments quantities directly related to the orientation parameters of single molecules. This derivation shows that provided that the incident polarization state and the rotational rate of molecules is known in the medium of study, orientational parameters can be retrieved in an accurate manner in SMOLM techniques that generally allow retrieval of dipole moment quantities. This study shows that in most of the situations where wobbling is present over a large angular extent δ, unknown polarization state of the excitation can provoke important bias in the determination of the orientation parameters of single molecules, in situations where the rotational diffusion time is shorter than the fluorescence lifetime. In general, lower wobbling extent are less strongly affected by such bias.

At last, while an ideal isotropic incoherent excitation field is delicate to obtain, situations where the rotational rate is much faster than the fluorescence lifetime ensures accurate determination of angular single molecule parameters. In such situation in the presence of very small wobbling angles however, a possible photoselection can occur from the angular dependence of the absorption probability, making the process sensitive to certain orientations only.

Acknowledgements

This research has received funding from the « Investissements d'Avenir » French Government program managed by the French National Research Agency ANR (ANR-16-CONV-0001), from the France BioImaging National Infrastructure (ANR-10-INBS-04), from CNRS (MITI «Lumière et vie -2022»), from the European Union's Horizon 2020 research and innovation programme under grant agreement No 812922, and from the 3DPolariSR ANR grant (ANR-20-CE42-0003).

References

1. Stallinga, S., Rieger, B., Betzig, E., Patterson, G.H., Sougrat, R., Lindwasser, O.W., Olenych, S., Bonifacino, J.S., Davidson, M.W., Lippincott-Schwartz, J., Hess, H.F., Schüttpelz, M., Kasper, R., Seefeldt, B., Mukherjee, A., Tinnefeld, P., and Sauer, M. (2012) Position and orientation estimation of fixed dipole emitters using an effective Hermite point spread function model. *Opt. Express, Vol. 20, Issue 6, pp. 5896-5921*, **20** (6), 5896–5921.

2. Backlund, M.P., Lew, M.D., Backer, A.S., Sahl, S.J., and Moerner, W.E. (2014) The role of molecular dipole orientation in single-molecule fluorescence microscopy and implications for super-resolution imaging. *ChemPhysChem*, **15** (4), 587–599.

3. Backer, A.S., and Moerner, W.E. (2015) Determining the rotational mobility of a single molecule from a single image: a numerical study. *Opt. Express*, **23** (4), 4255.

4. Backer, A.S., Backlund, M.P., Lew, M.D., and Moerner, W.E. (2013) Single-molecule orientation measurements with a quadrated pupil. *Opt. Lett.*, **38** (9), 1521.

5. Lew, M.D., Zhang, O., Lew, M.D., and Lew, M.D. (2021) Single-molecule orientation localization microscopy II: a performance comparison. *JOSA A, Vol. 38, Issue 2, pp. 288-297*, **38** (2), 288–297.

6. Sahu, S.P., Mahigir, A., Chidester, B., Veronis, G., and Gartia, M.R. (2019) Ultrasensitive Three-Dimensional Orientation Imaging of Single Molecules on Plasmonic Nanohole Arrays Using Second Harmonic Generation. *Nano Lett.*, **19** (9), 6192–6202.

7. Lakowicz, J.R. (1999) Principles of Fluorescence Spectroscopy. *Princ. Fluoresc. Spectrosc.*

8. Börner, R., Ehrlich, N., Hohlbein, J., and Hübner, C.G. (2016) Single Molecule 3D Orientation in Time and Space: A 6D Dynamic Study on Fluorescently Labeled Lipid Membranes. *J. Fluoresc.*, **26** (3), 963–975.

9. Iniesta, A., and García de la Torre (1987) Rotational diffusion coefficients of a small, spherical subunit flexibly tethered to a larger sphere. *Eur. Biophys. J.*, **14** (8), 493–498.

10. Börner, R., Kowerko, D., von Borczyskowski, C., and Hübner, C.G. (2011) Time resolved 3D orientation spectroscopy: experimental realization and simulation. *Single Mol. Spectrosc. Imaging IV*, **7905**, 79050D.

11. Oura, M., Yamamoto, J., Ishikawa, H., Mikuni, S., Fukushima, R., and Kinjo, M. (2016) Polarization-dependent fluorescence correlation spectroscopy for studying structural properties of proteins in living cell. *Sci. Reports 2016 61*, **6** (1), 1–7.

12. Lew, M.D., Backlund, M.P., and Moerner, W.E. (2013) Rotational Mobility of Single Molecules

Affects Localization Accuracy in Super-Resolution Fluorescence Microscopy. *Nano Lett.*, **13** (9), 3967–3972.

13. Zhang, O., Lu, J., Ding, T., and Lew, M.D. (2018) Imaging the three-dimensional orientation and rotational mobility of fluorescent emitters using the Tri-spot point spread function. *Appl. Phys. Lett.*, **113** (3), 031103.

14. Zhang, O., Zhou, W., Lu, J., Wu, T., and Lew, M.D. (2022) Resolving the Three-Dimensional Rotational and Translational Dynamics of Single Molecules Using Radially and Azimuthally Polarized Fluorescence. *Nano Lett.*, **22** (3), 1024–1031.

15. Stallinga, S. (2015) Effect of rotational diffusion in an orientational potential well on the point spread function of electric dipole emitters. *JOSA A, Vol. 32, Issue 2, pp. 213-223*, **32** (2), 213–223.

16. Valades Cruz, C.A., Shaban, H.A., Kress, A., Bertaux, N., Monneret, S., Mavrakis, M., Savatier, J., and Brasselet, S. (2016) Quantitative nanoscale imaging of orientational order in biological filaments by polarized superresolution microscopy. *Proc. Natl. Acad. Sci. U. S. A.*, **113** (7), E820–E828.

17. Rimoli, C.V., Valades-Cruz, C.A., Curcio, V., Mavrakis, M., and Brasselet, S. (2022) 4polar-STORM polarized super-resolution imaging of actin filament organization in cells. *Nat. Commun. 2022 131*, **13** (1), 1–13.

18. Backlund, M.P., Lew, M.D., Backer, A.S., Sahl, S.J., Grover, G., Agrawal, A., Piestun, R., and Moerner, W.E. (2012) Simultaneous, accurate measurement of the 3D position and orientation of single molecules. *Proc. Natl. Acad. Sci. U. S. A.*, **109** (47), 19087–92.

19. Ding, T., Wu, T., Mazidi, H., Zhang, O., and Lew, M.D. (2020) Single-molecule orientation localization microscopy for resolving structural heterogeneities between amyloid fibrils. *Optica*, **7** (6), 602.

20. Hulleman, C.N., Thorsen, R.Ø., Kim, E., Dekker, C., Stallinga, S., and Rieger, B. (2021) Simultaneous orientation and 3D localization microscopy with a Vortex point spread function. *Nat. Commun. 2021 121*, **12** (1), 1–14.

21. Curcio, V., Brown, T.G., Brasselet, S., and Alonso, M.A. (2019) Birefringent Fourier filtering for single molecule Coordinate and Height super-resolution Imaging with Dithering and Orientation (CHIDO). *Nat. Commun. 2020 111*, **11** (1), 1–13.

22. Kinosita, K., Kawato, S., and Ikegami, A. (1977) A theory of fluorescence polarization decay in membranes. *Biophys. J.*, **20** (3), 289–305.

23. Florine-Casteel, K. (1990) Phospholipid order in gel- and fluid-phase cell-size liposomes measured by digitized video fluorescence polarization microscopy. *Biophys. J.*, **57** (6), 1199–215.

24. Axelrod, D. (2008) Chapter 7 Total Internal Reflection Fluorescence Microscopy. *Methods Cell Biol.*, **89**, 169–221.

25. Adamczyk, A.K., Huijben, T.A.P.M., Sison, M., Di Luca, A., Chiarelli, G., Vanni, S., Brasselet, S., Mortensen, K.I., Stefani, F.D., Pilo-Pais, M., and Acuna, G.P. (2022) DNA Self-Assembly of Single Molecules with Deterministic Position and Orientation. *ACS Nano*, **16** (10), 16924–16931.

26. Hohlbein, J., and Hübner, C.G. (2005) Simple scheme for rapid three-dimensional orientation determination of the emission dipole of single molecules. *Appl. Phys. Lett.*, **86** (12), 121104.